

Visualising Information Flow in Word Embeddings with Diffusion Tensor Imaging

Thomas Fabian

Technical University Darmstadt

thomas.fabian@tu-darmstadt.de

Abstract

Understanding how large language models (LLMs) represent natural language is a central challenge in natural language processing (NLP) research. Many existing methods extract word embeddings from an LLM, visualise the embedding space via point-plots, and compare the relative positions of certain words. However, this approach only considers single words and not whole natural language expressions, thus disregards the context in which a word is used. Here we present a novel tool for analysing and visualising information flow in natural language expressions by applying diffusion tensor imaging (DTI) to word embeddings. We find that DTI reveals how information flows between word embeddings. Tracking information flows within the layers of an LLM allows for comparing different model structures and revealing opportunities for pruning an LLM’s under-utilised layers. Furthermore, our model reveals differences in information flows for tasks like pronoun resolution and metaphor detection. Our results show that our model permits novel insights into how LLMs represent actual natural language expressions, extending the comparison of isolated word embeddings and improving the interpretability of NLP models.

1 Introduction

Modern natural language processing (NLP) models, or large language models (LLMs), depend on representations of words in high-dimensional embedding spaces. LLMs generate a high-dimensional word embedding with rich linguistic information for every word in natural language. However, interpreting the information captured in these embeddings is challenging because individual dimensions lack intuitive meaning (Bender and Koller, 2020), and the process of learning these representations from large amounts of textual data remains opaque (Lipton, 2018; Rudin, 2019). Thus, enhancing the interpretability of NLP models has

become a scientific endeavour of its own, whose goals are understanding how LLMs represent linguistic information and decoding this information. To better understand and control artificial intelligence, especially for building trust in these models and ensuring their responsible deployment, it is essential to understand how information is represented in LLMs. To achieve this, there are numerous approaches for visualising high-dimensional embeddings of LLMs.

Existing visualisations of word embeddings (Ahlberg and Shneiderman, 1994; Weaver, 2004; van der Maaten and Hinton, 2008; Smilkov et al., 2016; McInnes et al., 2020) can be used to compare the locations of words in the embedding space, or to find the nearest neighbours or semantic clusters. These relational connections between word embeddings can provide valuable insights into how LLMs represent information, such as the fact that subtracting the embedding for *man* from the embedding for *woman* reveals a direction vector encoding femininity in the embedding space (Mikolov et al., 2013). Similarly, semantic clusters can be identified by preserving local neighbourhoods through algorithms such as t-SNE (van der Maaten and Hinton, 2008), while manifold methods such as UMAP (McInnes et al., 2020) retain more structural details in the low-dimensional layout.

However, these visualisation methods exhibit two major shortcomings. First, in the plots they create, the axes do not have any intuitive meaning due to the dimensionality reduction from the high-dimensional embedding space to only a few dimensions suitable for visualisation. Thus, statements about embedding spaces rest on linear projections or scatter plots that can only be interpreted by taking relative positions into account. Second, existing visualisation methods can only compare the embeddings of isolated words, without providing insights into how information representations vary in the context of actual expressions of syntac-

tically and semantically connected words. Hence, they cannot visualise the information flow between words in a sentence as it occurs in natural language.

In the field of neuroscience, visualising flows of liquids is well established, as diffusion tensor imaging (DTI) has been used for decades to visualise diffusivity in the human brain (Basser et al., 1994; LeBihan et al., 2001; Westin et al., 2002). The idea behind DTI is to calculate a 3×3 diffusion tensor around each voxel, which is then visualised using a diffusion ellipsoid. The lengths of the ellipsoid axes show the strength and direction of water diffusivity in tissue. In this context, isotropic diffusion refers to diffusivity being equally strong in all directions, while anisotropic diffusion denotes the diffusion being stronger along one axis than along the other axes. Since water diffusivity, or flow, is highest along the primary fibre direction, the direction of the anisotropic diffusion ellipsoids indicates the alignment of fibres in the brain. More notably, DTI not only allows for investigating diffusivity in the brains of healthy individuals, but is also particularly useful for investigating which alterations of diffusivity occur when people suffer from brain disorders (Pini et al., 2016; Arbabshirani et al., 2017; Wood et al., 2024).

As with the human brain, understanding the activities of individual structures in LLMs can help identify the integral components and underutilised parts of the system. In NLP research, the goal of structured pruning, i.e., the removal of redundant parameters or superfluous components of a neural network, is to reduce model complexity with as little performance loss as possible (LeCun et al., 1989; Hassibi et al., 1993). Effective pruning of NLP models is of considerable practical importance, as operating a model after training, known as inference, accounts for approximately 60–70% of an LLM’s computing and energy requirements (Patterson et al., 2022; Wu et al., 2022; Desislavov et al., 2023; Mavromatis et al., 2024). Numerous studies introduce methods for reducing the model complexity of LLMs, among other things, to reduce the computational effort and energy requirements during inference (Teerapittayanon et al., 2016; Fan et al., 2019; Blalock et al., 2020; Xia et al., 2022; Tao et al., 2023; Varshney et al., 2024). In this context, metrics of the information flow through an LLM’s layers could be used to reveal the need for pruning or to optimise pruning methods by indicating remaining inefficiencies or explaining performance losses.

Based on DTI and its capability of highlighting alterations of flow, we propose a novel visualisation method to depict directional relations between word embeddings, indicating the information flow in natural language expressions of any length. To evaluate information flow via diffusion ellipsoids, we propose a tool for **Diffusion-Oriented Natural-language Anisotropy and Layer-wise Directionality Diagnostics** (DONALD-D). We visualise the flow of information through the words of a sentence using diffusion ellipsoids, which we calculate based on word embeddings. DONALD-D rests on the idea of concatenating the embeddings of words in a sentence to a two-dimensional matrix, applying DTI to calculate structure tensors within this matrix, and visualising the information flow across words with diffusion ellipsoids. With this procedure, DONALD-D transforms abstract embedding patterns into human-interpretable images of information flow within natural language expressions of any length.

The contribution of this work is the introduction of a novel visualisation method for LLMs’ embedding spaces based on diffusion ellipsoids. DONALD-D leverages the interpretability of DTI to visualise the information flow between words in the context of natural language expressions, a relationship that cannot be visualised using existing methods. The model thus offers two improvements over existing visualisations: first, the axes of the visualisation can be interpreted quite intuitively, and second, the relationships between embeddings can be visualised in the actual context of real natural language expressions. Due to its direct applicability to natural language expressions of any length, DONALD-D allows for new investigations into the structure of LLM embedding spaces. By enabling the assessment of layer utilisation in embedding spaces, DONALD-D allows the identification of opportunities to prune individual under-utilised layers within an LLM or explain why a pruned model loses performance. At the same time, understanding the information flows that LLMs capture during training on natural language data might allow insights into human language use and the functions of individual words.¹

¹The code for DONALD-D is publicly available at https://osf.io/rc3ts/overview?view_only=ab167d7a24be4e678a7ad0f4d0dd0e12

2 Methods

2.1 Input processing

DONALD-D operates with any common hidden-state format used in LLMs. The numbers of layers L , tokens T , and hidden units H usually form an embedding space as stacked layer arrays or per-token stacks with shapes (L, T, H) and (T, L, H) , respectively. This applies to all models available on Hugging Face (Wolf et al., 2020). For unconventionally shaped embedding spaces, DONALD-D includes an automated layout detection by axis sizes. Although DONALD-D can process all embeddings, we focus on the transformer-block outputs and exclude the embedding output as it encodes conceptually different information (Ethayarajh, 2019; Tenney et al., 2019). Note that for one sentence, the number of tokens T can vary between models as the tokenisation processes differ. The first transformation is collapsing the hidden-unit axis H by an arithmetic mean for layer $i \in \{0, \dots, L-1\}$ and token $j \in \{0, \dots, T-1\}$:

$$M_{i,j} = \frac{1}{H} \sum_{h=1}^H E_{i,j,h}. \quad (1)$$

This yields a matrix $M \in \mathbb{R}^{L \times T}$ containing one value for each layer-token combination. Despite losing information, we opt for the arithmetic mean as the individual values of hidden units are not intuitively interpretable. Visualising the hidden units would be possible with DTI. However, adding hidden units would not improve the interpretability of the visualisations and impair readability due to overloading and introducing the general ambiguities in three-dimensional visualisations (Tufte, 1983; Cleveland and McGill, 1984). Furthermore, we decide against principal component analysis for dimension reduction, as the results would be rendered intuitively uninterpretable.

After collapsing the hidden units, we apply row-wise min-max normalisation to better compare information flow within layers and between tokens. By applying min–max normalisation per each row i

$$M_{i,\cdot} = \frac{M_{i,\cdot} - \min_j M_{i,j}}{\max_j M_{i,j} - \min_j M_{i,j}} \quad (2)$$

the values of each row are normalised to the interval $[0, 1]$. By equalising the range of each layer, the

resulting tensors become comparable across layers even if one layer has systematically larger values than another. In combination with the preserved token-wise variation, the calculated anisotropy is comparable between layers, yet sensitive to variations between tokens, serving the goal of visualising information flow in natural language.

For completeness and possible other applications, DONALD-D also provides options for column-wise and global min-max normalisation prior to gradient estimation, but both impair the visualisation and detectability of information flow. Column-wise min-max normalisation removes cross-token variations, i.e., information flow, altogether. Global normalisation minimises contrast as outliers dominate the normalisation interval, compressing the remaining matrix entries into a narrow range of values. In the subsequent gradient estimation, these similar values result in small gradients and near-isotropic tensors across the entire matrix, rendering the detection of information flow impossible.

2.2 Structure tensor estimation

To estimate the structure tensors, we first determine the gradients in matrix M . DONALD-D calculates the gradients $\partial_x M$ (horizontal/token-to-token) and $\partial_y M$ (vertical/layer-to-layer) as discrete spatial derivatives on the basis of centred finite differences. As the previous normalisations yield unit grid spacing for matrix M , we can compute its derivative fields element-wise as

$$\partial_x M_{i,j} = \frac{M_{i,j+1} - M_{i,j-1}}{2}, \quad (3)$$

$$\partial_y M_{i,j} = \frac{M_{i+1,j} - M_{i-1,j}}{2}. \quad (4)$$

Next, we apply Gaussian smoothing to the derivative fields to reduce noise sensitivity in the separately calculated derivatives. The smoothing is implemented as a convolution of each derivative field, $\partial_x M$ and $\partial_y M$, with an isotropic Gaussian kernel. For applications that require stronger smoothing along either layers or tokens, an anisotropic smoothing kernel can be applied at this point. The derivative fields for the horizontal and vertical gradients are used to calculate the raw second-moment components

$$J_{xx} = (\partial_x M)^2, \quad (5)$$

$$J_{xy} = (\partial_x M)(\partial_y M), \quad (6)$$

$$J_{yx} = (\partial_y M)(\partial_x M), \quad (7)$$

$$J_{yy} = (\partial_y M)^2, \quad (8)$$

which indicate directional change, or flow, across the horizontal, vertical, and diagonal axes. We apply Gaussian smoothing to stabilise the noise-sensitive raw second-moment components and obtain the coherent local directionality of neighbourhoods.

Lastly, the structure tensors are assembled from the smoothed second-moment components. Each cell of the initial token-layer matrix M can be represented as a combination of the directional flows through it. For each cell, the information flow is captured in a symmetric 2×2 structure tensor

$$\mathbf{J}_{i,j} = \begin{pmatrix} J_{xx}(i,j) & J_{xy}(i,j) \\ J_{yx}(i,j) & J_{yy}(i,j) \end{pmatrix} + \varepsilon I, \quad (9)$$

with $\varepsilon = 10^{-12}$ added to ensure numerical stability. With this procedure, DONALD-D performs a numerically stable estimation of structure tensors that capture the local pattern of information flow for each token-layer combination of the LLM's embedding space. Although the pattern of information flow is calculated locally, it depends on the whole input as transformer models are based on the idea of every input paying attention to all other inputs (Vaswani et al., 2017). Thus, if words are added to the end of a sentence, the first tokens' representations in the embedding space will change to capture the new context. One could calculate the structure tensors for longer sequences but we suspect the added insight to be limited as long-range dependencies between tokens are already part of a token's embedding space representation.

With the tensor components $J_{xx}(i,j)$ and $J_{yy}(i,j)$, we also determine the utilisation rate of every layer, i.e., the fraction of information diffusion along the token-to-token direction, as

$$U_i = \frac{1}{N} \sum_{j=1}^N \frac{J_{xx}(i,j)}{J_{xx}(i,j) + J_{yy}(i,j) + \varepsilon}, \quad (10)$$

with $\varepsilon = 10^{-12}$ for avoiding division by zero. For every layer, the utilisation rate U denotes the

average fraction of diffusion between tokens. A low utilisation rate indicates little change across tokens within a layer. Thus, it suggests that the respective layer might be redundant in the embedding space as differences between tokens are captured by other layers.

2.3 Anisotropy calculation

Calculating the anisotropy of each cell in matrix M necessitates the eigen-decomposition of each local structure tensor \mathbf{J} as

$$\mathbf{J}_{i,j} v_k(i,j) = \lambda_k(i,j) v_k(i,j), \quad (11)$$

with $k = 1, 2$. Diagonalising structure tensor $\mathbf{J}_{i,j}$ yields the eigenvectors $v_1(i,j)$ and $v_2(i,j)$, from which the principal eigenvector $v_1(i,j)$ indicates the dominant direction of local flow, and the eigenvalues $\lambda_1(i,j) \geq \lambda_2(i,j)$, which quantify the amount of energy aligned with each direction. From the eigenvalues, we calculate the degree of anisotropy following established practice (Bigun and Granlund, 1987; Weickert, 1999) as

$$A(i,j) = \frac{\lambda_1(i,j) - \lambda_2(i,j)}{\lambda_1(i,j) + \lambda_2(i,j) + \varepsilon}, \quad (12)$$

with $\varepsilon = 10^{-12}$ avoiding division by zero. This normalised difference expresses the anisotropy in the interval $[0, 1]$, with $A = 0$ indicating no preferred direction, i.e., isotropy (Figure 1, left). Higher values suggest more anisotropic diffusion, with the information flow being more pronounced along one direction than the other (Figure 1, right).

By determining the eigenvectors and anisotropy, we obtain a principal vector field $v_1(x,y) : \{0, \dots, L-1\} \times \{0, \dots, T-1\} \rightarrow \mathbb{R}^2$ and the anisotropy scalar field $A(x,y) : \{0, \dots, L-1\} \times \{0, \dots, T-1\} \rightarrow [0, 1]$. Thus, for each combination of token and layer, DONALD-D provides the dominant direction as a two-dimensional vector and the fraction of energy that is applied to that direction.

This anisotropy measure is the two-dimensional analogue of fractional anisotropy (Basser et al., 1994), a three-dimensional anisotropy measure commonly used in DTI for neuroimaging. Alternative to our measure, one could determine anisotropy with different methods like tensor-shape decompositions (Westin et al., 2002) to capture the shape of diffusion with more detail. We opt for normalised

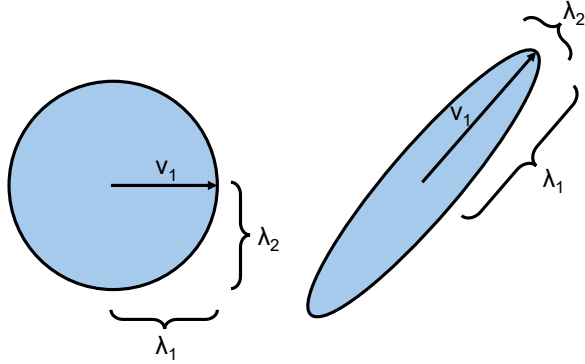


Figure 1: Isotropic (left) and anisotropic (right) diffusion. For isotropic diffusion, the eigenvalues λ_1 and λ_2 are equal. The degree of anisotropy increases with the difference between the eigenvalues as a larger fraction of directional strength runs along the principal eigenvector v_1 .

differences in DONALD-D to get a simple and intuitively interpretable visualisation of the structure tensors.

As the principal vector field and anisotropy scalar are calculated for each cell, they are only defined for the grid centres and can thus only be queried with integers. We included an interpolation so, technically, DONALD-D can be queried for principal flow direction and anisotropy at any continuous point within the matrix boundaries. However, as values off the grid centres lack interpretability, we focus on the discrete matrix structure to refer to distinct token-layer combinations.

2.4 Visualisation

We visualise the structure tensors as diffusion ellipsoids at the centre of every cell in the token-layer matrix. The ellipsoid is oriented in the direction of the principal eigenvector v_1 and its semi-axes are proportional to $\sqrt{\lambda_1}$ and $\sqrt{\lambda_2}$. Thus, each ellipsoid encodes the dominant direction and the directional strength, with a radially symmetric ellipsoid indicating isotropic diffusion. We apply a global scale factor to ensure that all ellipsoids fit into the corresponding matrix tile in the visualisation.

To visually highlight information flow directions, we colour the tiles of each token-layer combination according to their dominant direction of flow. The colourmap we apply is π -periodic, i.e., an angle θ is assigned the same colour as $\theta + 180^\circ$, as the calculated structure tensors do not indicate the direction of change. This property of DTI should pose no problem to the visualisation of information flow in natural language since all tokens have a

clearly defined sequence, leaving no possibility for information flowing backwards.

Given that all information must flow in the token sequence direction, we colour both diagonal axes identically as they equally reflect a deviation from the token-to-token information flow. Information flow running parallel to the token sequence is coloured red, diagonal deviations yellow, and flows perpendicular to the token sequence blue. To encode the directional strength in the colouring, the transparency of each tile is directly proportional to its degree of anisotropy. Thus, token-layer combinations with low directional strength, i.e., near-isotropic information diffusion, are visualised as almost white tiles.

The final visualisations created by DONALD-D thus comprise a colour-coded image of rectangular tiles, overlayed with ellipsoids encoding the directional strength of the local information diffusion. The colouring allows the plot to be read like a heatmap with red tiles indicating strong token-to-token changes within a layer and blue tiles indicating no information flow between tokens. The model’s parameters are set to balance the visualisation’s readability and the numerical accuracy. For other visualisation purposes, the parameters can be adjusted for optimal results. Concerning DONALD-D’s complexity, visualising how information flows through an LLM’s word embeddings scales linearly with the length of natural language expressions. Each processing step operates with independent 2×2 matrices that are calculated from matrix $M \in \mathbb{R}^{L \times T}$. As the number of layers L is constant for any given LLM, the complexity for analysing a natural language expression containing T tokens is $O(T)$.

2.5 Exemplary applications

For demonstrating how DONALD-D reveals model-dependent differences in information flow, we visualise the information flow in BERT (Devlin et al., 2019), Longformer (Beltagy et al., 2020), GPT-2 (Radford et al., 2019), and PEGASUS (Zhang et al., 2020) for a single exemplary sentence. These models represent a classical encoder-only model (BERT), an encoder-only model with sparse attention to capture long sequences (Longformer), a decoder-only model (GPT-2), and an encoder-decoder hybrid (PEGASUS). For this work, we use only license-free models available on Hugging Face (Wolf et al., 2020) to ensure unrestricted reproducibility. However, DONALD-D can be ap-

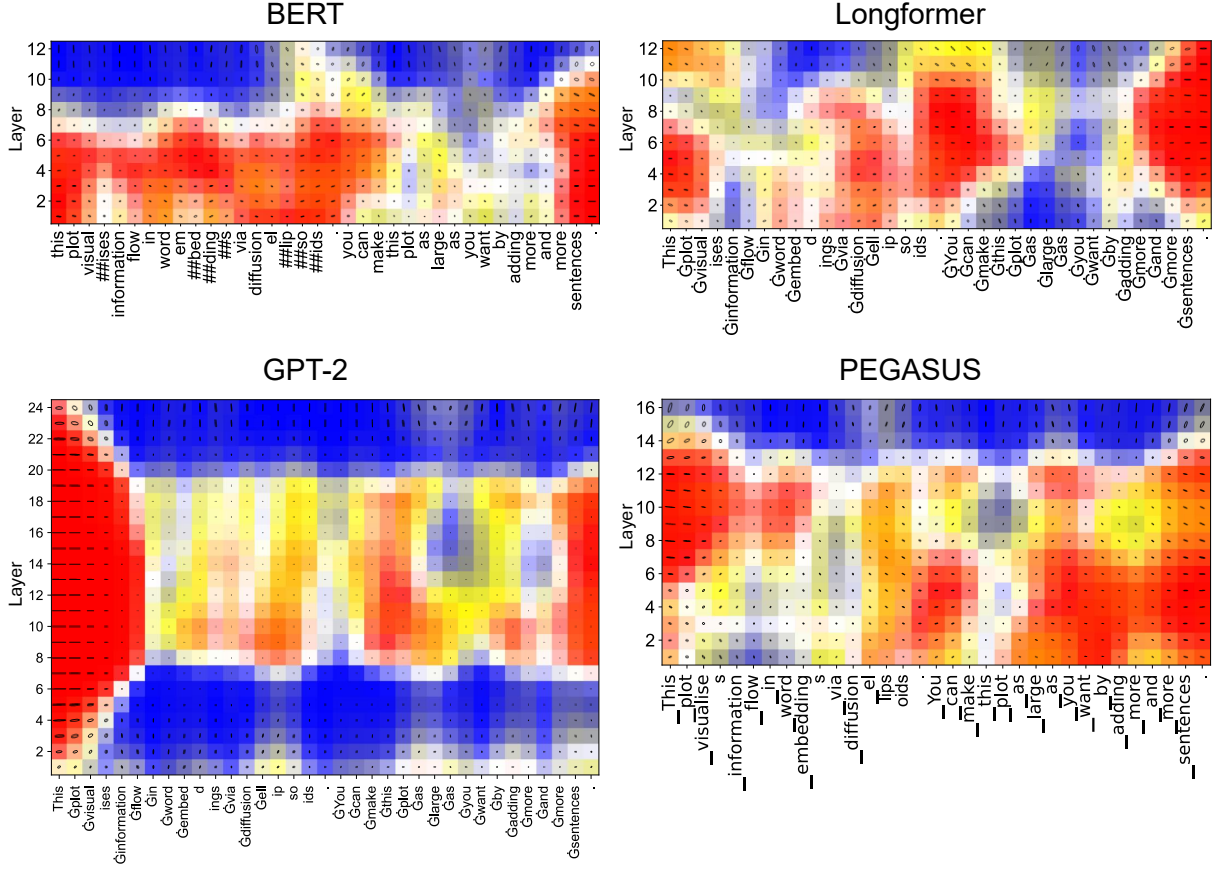


Figure 2: Information flow in an exemplary natural language expression in BERT (Devlin et al., 2019), Longformer (Beltagy et al., 2020), GPT-2 (Radford et al., 2019), and PEGASUS (Zhang et al., 2020). Each model tokenises and provides word embeddings for the expression: *This plot visualises information flow in word embeddings via diffusion ellipsoids. You can make this plot as large as you want by adding more and more sentences.* The x-axis shows the tokens, the number of which can vary between models due to different tokenisation processes. The y-axis shows the layers of each model. The ellipsoids within each tile encode the direction of information diffusion. Red tiles indicate token-to-token information flow. Blue tiles indicate no information flow along the token sequence.

plied to any LLM and any type of embedding as they all encode words as mathematical abstractions, whose concatenation can be examined for information flows via DTI.

Additionally, we use DONALD-D to investigate information flows for linguistic phenomena in BERT. The dimensions of BERT have been extensively studied (Rogers et al., 2020), which allows for a linguistic interpretation of the individual dimensions. Of BERT’s twelve layers, the first four dimensions encode semantic features, the central four dimensions represent syntactic features, and the last four dimensions capture surface features (Jawahar et al., 2019). Thus, information flows between tokens can be interpreted based on the layer in which they occur. We perform two exemplary minimal pair analyses to investigate how DONALD-D visualises context-dependent information flow changes. For pronoun resolution, we

use almost identical sentences in which only a pronoun differs. As an example of metaphor detection, we investigate the phrase *to kick the bucket* in a metaphorical and a literal context.

3 Results

We use DONALD-D to compare the information flow for the same exemplary input in four different LLMs (Figure 2) and quantitatively determine the utilisation rate per layer for each model (Appendix, Table 1).

The visualisations show how the two encoder-only models BERT and Longformer differ in their information flow (Figure 2, top). While BERT utilises layers one to eight the most, the last four layers only slightly change across most tokens. In Longformer, the same example sentence yields more evenly distributed information flows, with each section of the layers being utilised for cap-

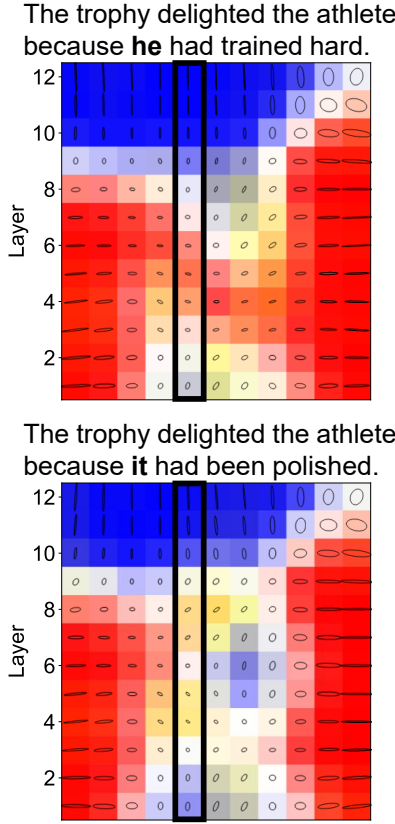


Figure 3: Minimal pair analysis for pronoun resolution. The word embeddings are taken from BERT (Devlin et al., 2019). Each column corresponds to a token in the expression. The highlighted columns correspond to the bold target words, *he* and *it*, respectively.

turing changes across tokens in different parts of the sentence. The utilisation rates deliver similar results as they more evenly distributed across layers in Longformer (mean = 54.94%, SD = 11.37%) than BERT (mean = 50.63%, SD = 27.35%).

For the decoder-only model GPT-2 (Figure 2, bottom left), all layers display strong information diffusion along the first five tokens. However, from the sixth token onwards, the layers’ utilisation shows pronounced differences. Layers one to seven and twenty to twenty-four show little information flow, as more than two-thirds of the information diffuses perpendicular to the token sequence. Layers eight to nineteen exhibit the majority of changes between tokens, indicating that it is mainly these layers that allow the model to distinguish one token’s representation from the surrounding tokens. For GPT-2, the utilisation varies by layer, similar to BERT, but the average layer-utilisation is considerably lower than for the encoder-only models (mean = 40.90%, SD = 25.13%).

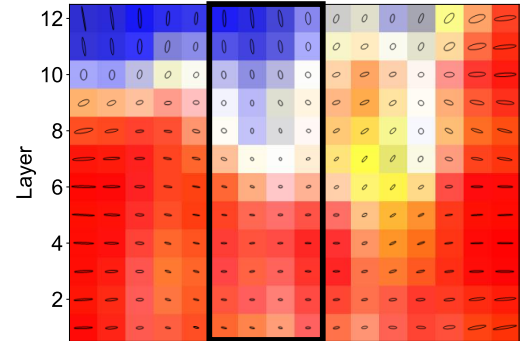
The encoder-decoder model PEGASUS (Fig-

ure 2, bottom right) shows information flows similar to those of BERT (Figure 2, top left), with the highest layers being under-utilised. The average utilisation rate per layer and the deviation by layer in PEGASUS also appear similar to the encoder-only models (mean = 56.18%, SD = 23.53%).

To see how different phenomena of natural language are represented in an LLM, we visualise the information flow in BERT for different sentences. First, we visualise how the information flow in BERT changes during pronoun resolution (Figure 3).

The most distinct information flow differences between the pronouns occur in layers three to six. This indicates that the pronoun resolution does not involve the surface-level features but a combination of semantic and syntactic features. The information flows left of the target pronouns also change with the pronoun, showing how the word embeddings for tokens in a sentence change when others are replaced. This indicates that DONALD-D is, despite its local diffusion ellipsoid evaluation, capable of

After decades of illness, **he kicked the bucket**. It was a sad day.



After the match, **he kicked the bucket** into the corner. It was a sad day.

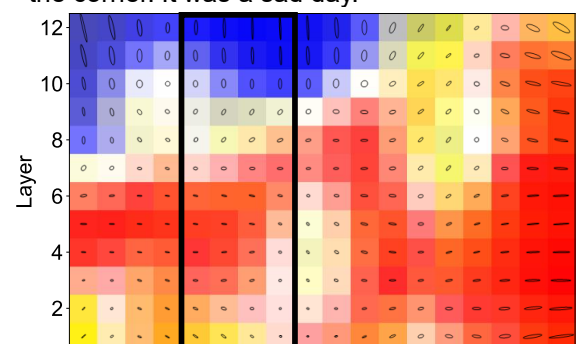


Figure 4: Minimal pair analysis for metaphor detection. The word embeddings are taken from BERT (Devlin et al., 2019). Each column corresponds to a token in the expression, highlighted columns correspond to the bold target phrase *he kicked the bucket*.

capturing long-range dependencies via the LLM’s word embeddings.

As another phenomenon, we visualise how metaphorical expressions alter the information flow (Figure 4). For the metaphorical use of the expression, the information flow in the lower layers is more pronounced than in the literal use. As the lower layers capture semantic information, this indicates that the semantic token-to-token differences increase when the expression is used metaphorically.

4 Discussion

In this work, we use diffusion tensor imaging to visualise information flow between tokens in natural language expressions. The differences in information flow patterns between LLMs show how representations of natural language expressions differ from model to model. Even for models with comparable architectures, like the encoder-only models BERT and Longformer, DONALD-D reveals differences in the embedding space. In the case of BERT, for which the function of different layer sections is established (Jawahar et al., 2019), DONALD-D shows how the highest four layers capture surface features like punctuation, as only for these tokens there is a token-to-token information flow.

We provided examples of how DONALD-D can be used for calculating the structure tensors of information flow in word embeddings and visualising these flows. Corpus-based analyses would be needed to make statements about the actual utilisation rates of the LLMs’ layers. Systematic analyses with large corpora of natural language could reveal if an LLM exhibits only little information flow within certain layers of its embedding space. Such a result would suggest pruning as we consider it reasonable to assume that removing under-utilised layers from a model should have little impact on its performance. Under-utilised layers contain similar information for each token, rendering their contained information redundant and their presence in the model superfluous.

The utilisation rate of layers could also be analysed in a domain- and task-specific manner (Zhao et al., 2025). Using DONALD-D and a specialised corpus, one could determine which layers of an LLM are under-utilised in a specific use-case, which would indicate an opportunity for pruning based on **Diffusivity Under Context Knowledge** (DUCK). DUCK-pruning the main LLM accord-

ing to the layers’ utilisation rates would yield an arbitrary number of smaller models without the need for retraining. The DUCK-pruned models would be tailored to the specific task with minimal performance loss and, compared to the main model, computationally less demanding and less energy-consuming during inference.

The results for the exemplary language phenomena show that information flows differ with language use. Understanding how information flows differ for natural language phrases in certain contexts could help improve an LLM’s performance on tasks like pronoun resolution or metaphor detection. DONALD-D could reveal systematic deviations in information flows for certain contexts, e.g., metaphorical language use. Uncovering such patterns would allow us to understand why a model might fail to resolve the context-dependent variation in meaning and also to improve the performance of LLMs by providing them with additional information for context resolution.

DONALD-D provides an extension of the existing point-plot visualisations. Established visualisations of word embeddings do not consider the context in which a word is used. The average meaning extracted by an LLM is plotted together with other words’ embeddings and their relative positions might reveal systematic differences in how an LLM represents meaning (Mikolov et al., 2013). With DONALD-D, the information flow between word embeddings can be visualised for actual natural language expressions. This visualisation provides insights into how an LLM’s word embeddings function within the context of natural language. Thus, DONALD-D presents a novel visualisation and analysis method that can enhance the interpretability of LLMs, reveal opportunities for pruning, and allow for new LLM-based linguistic analyses. We hope that our work will open up a new avenue for the analysis and understanding of LLMs.

Limitations

DONALD-D collapses the hidden units of each layer and only considers the arithmetic mean. This simplification allows for clear visualisations that are interpretable. However, collapsing the hidden units into one value presents a simplification that potentially obscures changes in the hidden units as only their mean is considered. Especially for pruning, considering all the hidden layers separately

and creating three-dimensional diffusion models could provide more detailed information on the utilisation rates of an LLM’s layers.

The results described in this work are exemplary, as the main goal is to present a new visualisation and analysis tool. Large-scale corpus analyses are necessary to make robust statements about utilisation rates of LLMs or information flow patterns for specific language phenomena. As extensive corpus analyses are beyond the scope of this work, we leave them to future research.

References

Christopher Ahlberg and Ben Shneiderman. 1994. [Visual information seeking: tight coupling of dynamic query filters with starfield displays](#). In *Proceedings of the SIGCHI Conference on Human Factors in Computing Systems*, pages 313–317, Boston Massachusetts USA. ACM.

Mohammad R. Arbabshirani, Sergey Plis, Jing Sui, and Vince D. Calhoun. 2017. [Single subject prediction of brain disorders in neuroimaging: Promises and pitfalls](#). *Individual Subject Prediction*, 145:137–165.

Peter J. Basser, James Mattiello, and David LeBihan. 1994. [MR diffusion tensor spectroscopy and imaging](#). *Biophysical Journal*, 66(1):259–267. Publisher: Elsevier.

Iz Beltagy, Matthew E. Peters, and Arman Cohan. 2020. [Longformer: The Long-Document Transformer](#). *arXiv preprint*. ArXiv:2004.05150 [cs].

Emily M. Bender and Alexander Koller. 2020. [Climbing towards NLU: On Meaning, Form, and Understanding in the Age of Data](#). In *Proceedings of the 58th Annual Meeting of the Association for Computational Linguistics*, pages 5185–5198, Online. Association for Computational Linguistics.

Josef Bigun and Gösta H. Granlund. 1987. [Optimal Orientation Detection of Linear Symmetry](#). pages 433–438.

Davis Blalock, Jose Javier Gonzalez Ortiz, Jonathan Frankle, and John Gutttag. 2020. [What is the State of Neural Network Pruning?](#) *Proceedings of Machine Learning and Systems*, 2:129–146.

William S. Cleveland and Robert McGill. 1984. [Graphical Perception: Theory, Experimentation, and Application to the Development of Graphical Methods](#). *Journal of the American Statistical Association*, 79(387):531–554. Publisher: ASA Website.

Radosvet Desislavov, Fernando Martínez-Plumed, and José Hernández-Orallo. 2023. [Trends in AI inference energy consumption: Beyond the performance-vs-parameter laws of deep learning](#). *Sustainable Computing: Informatics and Systems*, 38:100857.

Jacob Devlin, Ming-Wei Chang, Kenton Lee, and Kristina Toutanova. 2019. [BERT: Pre-training of Deep Bidirectional Transformers for Language Understanding](#). In *Proceedings of the 2019 Conference of the North American Chapter of the Association for Computational Linguistics: Human Language Technologies, Volume 1 (Long and Short Papers)*, pages 4171–4186, Minneapolis, Minnesota. Association for Computational Linguistics.

Kawin Ethayarajh. 2019. [How Contextual are Contextualized Word Representations? Comparing the Geometry of BERT, ELMo, and GPT-2 Embeddings](#). *arXiv preprint*. ArXiv:1909.00512 [cs].

Angela Fan, Edouard Grave, and Armand Joulin. 2019. [Reducing Transformer Depth on Demand with Structured Dropout](#). *arXiv preprint*. ArXiv:1909.11556 [cs].

Babak Hassibi, David G. Stork, and Greg J. Wolff. 1993. [Optimal Brain Surgeon and general network pruning](#). In *IEEE International Conference on Neural Networks*, pages 293–299.

Ganesh Jawahar, Benoît Sagot, and Djamé Seddah. 2019. [What Does BERT Learn about the Structure of Language?](#) In *Proceedings of the 57th Annual Meeting of the Association for Computational Linguistics*, pages 3651–3657, Florence, Italy. Association for Computational Linguistics.

Denis LeBihan, Jean-François Mangin, Cyril Poupon, Chris A. Clark, Sabina Pappata, Nicolas Molko, and Hughes Chabriat. 2001. [Diffusion tensor imaging: Concepts and applications](#). *Journal of Magnetic Resonance Imaging*, 13(4):534–546. Publisher: John Wiley & Sons, Ltd.

Yann LeCun, John Denker, and Sara Solla. 1989. [Optimal Brain Damage](#). In *Advances in Neural Information Processing Systems*, volume 2, pages 598–605. Morgan-Kaufmann.

Zachary C. Lipton. 2018. [The Mythos of Model Interpretability: In machine learning, the concept of interpretability is both important and slippery](#). *Queue*, 16(3):31–57.

Ioannis Mavromatis, Kostas Katsaros, and Aftab Khan. 2024. [Computing Within Limits: An Empirical Study of Energy Consumption in ML Training and Inference](#). *arXiv preprint*. ArXiv:2406.14328 [cs].

Leland McInnes, John Healy, and James Melville. 2020. [UMAP: Uniform Manifold Approximation and Projection for Dimension Reduction](#). *arXiv preprint*. ArXiv:1802.03426 [stat].

Tomas Mikolov, Kai Chen, Greg Corrado, and Jeffrey Dean. 2013. [Efficient Estimation of Word Representations in Vector Space](#). *arXiv preprint*. ArXiv:1301.3781 [cs].

David Patterson, Joseph Gonzalez, Urs Hözle, Quoc Le, Chen Liang, Lluis-Miquel Munguia, Daniel Rothchild, David R. So, Maud Texier, and Jeff Dean. 2022. [The Carbon Footprint of Machine Learning Training Will Plateau, Then Shrink](#). *Computer*, 55(7):18–28.

Lorenzo Pini, Michela Pievani, Martina Bocchetta, Daniele Altomare, Paolo Bosco, Enrica Cavedo, Samantha Galluzzi, Moira Marizzoni, and Giovanni B. Frisoni. 2016. [Brain atrophy in Alzheimer’s Disease and aging](#). *Brain Imaging and Aging*, 30:25–48.

Alec Radford, Jeffrey Wu, Rewon Child, David Luan, Dario Amodei, and Ilya Sutskever. 2019. Language models are unsupervised multitask learners. *OpenAI blog*, 1(8):9.

Anna Rogers, Olga Kovaleva, and Anna Rumshisky. 2020. [A Primer in BERTology: What We Know About How BERT Works](#). *Transactions of the Association for Computational Linguistics*, 8:842–866. Place: Cambridge, MA Publisher: MIT Press.

Cynthia Rudin. 2019. Stop explaining black box machine learning models for high stakes decisions and use interpretable models instead. *Nature Machine Intelligence*, 1(5):206–215.

Daniel Smilkov, Nikhil Thorat, Charles Nicholson, Emily Reif, Fernanda B. Viégas, and Martin Wattenberg. 2016. [Embedding Projector: Interactive Visualization and Interpretation of Embeddings](#). *arXiv preprint*. ArXiv:1611.05469 [stat].

Chaofan Tao, Lu Hou, Haoli Bai, Jiansheng Wei, Xin Jiang, Qun Liu, Ping Luo, and Ngai Wong. 2023. [Structured Pruning for Efficient Generative Pre-trained Language Models](#). In *Findings of the Association for Computational Linguistics: ACL 2023*, pages 10880–10895, Toronto, Canada. Association for Computational Linguistics.

Surat Teerapittayanon, Bradley McDanel, and Hsiang Tsung Kung. 2016. [BranchyNet: Fast inference via early exiting from deep neural networks](#). In *2016 23rd International Conference on Pattern Recognition (ICPR)*, pages 2464–2469.

Ian Tenney, Patrick Xia, Berlin Chen, Alex Wang, Adam Poliak, R. Thomas McCoy, Najoung Kim, Benjamin Van Durme, Samuel R. Bowman, Dipanjan Das, and Ellie Pavlick. 2019. [What do you learn from context? Probing for sentence structure in contextualized word representations](#). *arXiv preprint*. ArXiv:1905.06316 [cs].

Edward R Tufte. 1983. *The visual display of quantitative information*. Graphics Press USA, Cheshire, CT. Issue: 9.

Laurens van der Maaten and Geoffrey Hinton. 2008. Visualizing data using t-SNE. *Journal of machine learning research*, 9(11):2579–2605.

Neeraj Varshney, Agneet Chatterjee, Mihir Parmar, and Chitta Baral. 2024. [Investigating Acceleration of LLaMA Inference by Enabling Intermediate Layer Decoding via Instruction Tuning with ‘LITE’](#). In *Findings of the Association for Computational Linguistics: NAACL 2024*, pages 3656–3677, Mexico City, Mexico. Association for Computational Linguistics.

Ashish Vaswani, Noam Shazeer, Niki Parmar, Jakob Uszkoreit, Llion Jones, Aidan N. Gomez, Łukasz Kaiser, and Illia Polosukhin. 2017. [Attention is All you Need](#). In *Advances in Neural Information Processing Systems*, pages 6000–6010.

Chris Weaver. 2004. [Building Highly-Coordinated Visualizations in Improvise](#). In *IEEE Symposium on Information Visualization*, pages 159–166. Journal Abbreviation: IEEE Symposium on Information Visualization.

Joachim Weickert. 1999. [Coherence-Enhancing Diffusion Filtering](#). *International Journal of Computer Vision*, 31(2):111–127.

Carl Fredrik Westin, Stephan E. Maier, Hatsuho Mammata, Arya Nabavi, Ferenc Andras Jolesz, and Ron Kikinis. 2002. [Processing and visualization for diffusion tensor MRI](#). *Medical Image Analysis*, 6(2):93–108.

Thomas Wolf, Lysandre Debut, Victor Sanh, Julien Chaumond, Clement Delangue, Anthony Moi, Pieric Cistac, Tim Rault, Remi Louf, Morgan Funtowicz, Joe Davison, Sam Shleifer, Patrick von Platen, Clara Ma, Yacine Jernite, Julien Plu, Canwen Xu, Teven Le Scao, Sylvain Gugger, and 3 others. 2020. [Transformers: State-of-the-Art Natural Language Processing](#). In *Proceedings of the 2020 Conference on Empirical Methods in Natural Language Processing: System Demonstrations*, pages 38–45, Online. Association for Computational Linguistics.

Kimberly H. Wood, Rodolphe Nenert, Aya M. Miften, George W. Kent, Madison Sleyster, Raima A. Memon, Allen Joop, Jennifer Pilkington, Adeel A. Memon, Riis N. Wilson, Corina Catul, Jerzy Szaflarski, and Amy W. Amara. 2024. [Diffusion Tensor Imaging-Along the Perivascular-Space Index Is Associated with Disease Progression in Parkinson’s Disease](#). *Movement Disorders*, 39(9):1504–1513. Publisher: John Wiley & Sons, Ltd.

Carole-Jean Wu, Ramya Raghavendra, Udit Gupta, Bilge Acun, Newsha Ardalani, Kiwan Maeng, Gloria Chang, Fiona Aga, Jinshi Huang, Charles Bai, Michael Gschwind, Anurag Gupta, Myle Ott, Anastasia Melnikov, Salvatore Candido, David Brooks, Geeta Chauhan, Benjamin Lee, Hsien-Hsin Lee, and 6 others. 2022. [Sustainable AI: Environmental Implications, Challenges and Opportunities](#). *Proceedings of Machine Learning and Systems*, 4:795–813.

Mengzhou Xia, Zexuan Zhong, and Danqi Chen. 2022. [Structured Pruning Learns Compact and Accurate](#)

Models. In *Proceedings of the 60th Annual Meeting of the Association for Computational Linguistics (Volume 1: Long Papers)*, pages 1513–1528, Dublin, Ireland. Association for Computational Linguistics.

Jingqing Zhang, Yao Zhao, Mohammad Saleh, and Peter Liu. 2020. **PEGASUS: Pre-training with Extracted Gap-sentences for Abstractive Summarization**. In *Proceedings of the 37th International Conference on Machine Learning*, pages 11328–11339. PMLR. ISSN: 2640-3498.

Yirao Zhao, Guizhen Chen, Kenji Kawaguchi, Lidong Bing, and Wenzuan Zhang. 2025. **Pruning General Large Language Models into Customized Expert Models**. *arXiv preprint*. ArXiv:2506.02561 [cs].

Appendix

The following table shows the utilisation rates of the four models BERT (Devlin et al., 2019), Longformer (LF; Beltagy et al., 2020), GPT-2 (Radford et al., 2019), and PEGASUS (Zhang et al., 2020) for an exemplary natural language expression.

Layer	BERT	LF	GPT-2	PEGASUS
24	-	-	7.02	-
23	-	-	8.70	-
22	-	-	10.68	-
21	-	-	14.07	-
20	-	-	26.05	-
19	-	-	55.47	-
18	-	-	63.03	-
17	-	-	58.47	-
16	-	-	57.75	4.55
15	-	-	61.14	7.70
14	-	-	62.93	17.39
13	-	-	62.89	41.87
12	7.57	34.56	66.44	71.36
11	11.07	40.12	73.26	73.08
10	16.80	48.51	77.93	65.45
9	24.84	56.29	75.24	62.29
8	38.83	60.34	64.87	66.31
7	59.85	64.38	30.81	72.85
6	75.10	67.10	15.83	72.90
5	77.28	69.61	13.05	68.79
4	75.62	66.78	12.42	69.35
3	76.26	59.53	13.82	73.30
2	74.24	49.87	19.28	69.08
1	70.06	41.34	30.48	62.67
Mean	50.63	54.94	40.90	56.18
SD	27.35	11.37	25.13	23.53

Table 1: Average fraction (in percent) of information diffusion distributed along the token-to-token direction for the expression visualised in Figure 2: *This plot visualises information flow in word embeddings via diffusion ellipsoids. You can make this plot as large as you want by adding more and more sentences.*